



## Development of chitosan-clay nanocomposite films from *Hermetia illucens*: analysis of chemical, physical, and mechanical properties

Dolores Ianniciello<sup>a</sup>, Ada Peláez Montosa<sup>b</sup>, Raquel de Melo Barbosa<sup>c</sup>, Fátima García Villén<sup>b</sup>, Rosanna Salvia<sup>a,d</sup>, Carmen Scieuzo<sup>a,d</sup>, César Viseras<sup>b,\*</sup>, Patrizia Falabella<sup>a,d,\*\*</sup>

<sup>a</sup> Department of Basic and Applied Sciences, University of Basilicata – Via dell'Ateneo Lucano 10, 85100 Potenza, Italy

<sup>b</sup> Department of Pharmacy and Pharmaceutical Technology, School of Pharmacy, University of Granada, Campus of Cartuja, 18071 s/n, Granada, Spain

<sup>c</sup> Department of Pharmacy and Pharmaceutical Technology, Universidad de Sevilla, C/Profesor García González 2, Seville 41012, Spain

<sup>d</sup> Spinoff XFlies s.r.l., University of Basilicata, Via dell'Ateneo Lucano 10, 85100 Potenza, Italy

### ARTICLE INFO

#### Keywords:

Biopolymers

Insects

*Hermetia illucens*

Chitosan

Clay

Wound healing

### ABSTRACT

Chitosan has gained great attention due to its properties. In this study, chitosan obtained from an innovative and sustainable source, the bioconverter insect *Hermetia illucens*, known as Black Soldier Fly (BSF), was used for the development of Chitosan-Clay Nanocomposite Films. Sepiolite and montmorillonite clays were used to produce the membranes. The interaction between insect-derived chitosan and clays was studied and the chemical, thermal, mechanical, and adhesive properties of the films were assessed. The incorporation of clays enhanced greater hydrophobicity than those made with commercial chitosan, particularly in unbleached samples. However, chitosan from *H. illucens* displayed lower elasticity and tensile strength. Despite this, the addition of clays to pupal exuviae and adult unbleached samples resulted in mechanical properties comparable to commercial chitosan. Adhesive properties of BSF chitosan consistently outperformed commercial chitosan. Unbleached samples demonstrated better performance, suggesting that the bleaching process is unnecessary for film production. Based on the results obtained, insect chitosan could be particularly advantageous in applications requiring improved adhesiveness and enhanced thermal resistance and hydrophobicity, such as in wound dressings for exudative wounds.

### 1. Introduction

The size of the global polymer market reached USD 716.83 billion in 2022 and is expected to increase at a Compound Annual Growth Rate (CAGR) of 5.4 % from 2023 to 2032, when it is expected to reach about USD 1207.11 billion [1]. The reason for this rapid growth is the need for environmentally sustainable products. In an effort to reduce waste and promote sustainability, there is an increasing trend to recycle polymeric materials and, at the same time, there is a growing demand for biopolymers [2]. Biodegradable polymers exhibit some advantages as they do not harm the environment and do not generate bioaccumulation, making them environmentally friendly. Using renewable resources, reducing greenhouse gas emissions, recovering by-products, and conserving fossil fuels are the main advantages of biopolymers [3].

Biodegradable polymers can be either natural or synthetically derived [4]. Natural polymers are derived from various resources including plants, fungi, animals, and microorganisms. Due to their presence in the tissues of living organisms, they are readily available and inexpensive. In addition, they have some important advantages including biodegradability, biocompatibility, and nontoxicity [5]. Polysaccharides are a group of biopolymers derived from natural sources that have potential applications in numerous fields. Although many of the biopolysaccharides, such as cellulose, originate from plants, they can also be derived from other sources, including animals, as do chitin and chitosan [6]. Chitin is a linear polymer consisting of *N*-acetyl-d-glucosamine (GlcNAc) repeating units; it is structurally similar to cellulose, but differs in the presence of acetamide groups on C2 [7,8]. Chitin is the main constituent of the exoskeleton of arthropods, but it is also an

\* Correspondence to: C. Viseras, Department of Pharmacy and Pharmaceutical Technology, School of Pharmacy, University of Granada, Campus of Cartuja, 18071 s/n, Granada, Spain.

\*\* Correspondence to: P. Falabella, Department of Basic and Applied Sciences, University of Basilicata – Via dell'Ateneo Lucano 10, 85100 Potenza, Italy.

E-mail addresses: [cviseras@ugr.es](mailto:cviseras@ugr.es) (C. Viseras), [patrizia.falabella@unibas.it](mailto:patrizia.falabella@unibas.it) (P. Falabella).

<https://doi.org/10.1016/j.ijbiomac.2025.143496>

Received 14 November 2024; Received in revised form 15 April 2025; Accepted 23 April 2025

Available online 28 April 2025

0141-8130/© 2025 The Authors. Published by Elsevier B.V. This is an open access article under the CC BY license (<http://creativecommons.org/licenses/by/4.0/>).

important component of the cell wall of fungi and yeasts. In each of these organisms, chitin plays a structural and tissue-protective function [9,10]. Because of its insolubility, to expand its range of utilization, chitin must be processed into more soluble derivatives, of which chitosan is the main one. Chitosan is obtained by removal of acetyl groups present on chitin, with formation of reactive amine groups, which can be protonated in aqueous solution. Indeed, chitosan is a polycation soluble in acidic solutions [10]. Chitosan offers advantages such as biodegradability, biocompatibility, antibacterial activity, gel-forming capacity, bioadhesive properties, and immunostimulatory effects [11]. Furthermore, chitosan can be processed into nanoparticles, gels, films, and fibrous matrices, significantly broadening its applicability across various scientific and industrial fields. This ability enhances drug release capabilities and enables diverse applications in medication delivery and biological processes compared to other biopolymers [12]. Chitosan naturally possesses intrinsic antibacterial activity, unlike other biopolymers such as alginate, collagen, and gelatin, which typically require chemical modifications or external agents to achieve antibacterial properties [13]. Its antibacterial properties are particularly advantageous in tissue regeneration and infection prevention [14]. This unique characteristic arises from its polycationic nature, which allows chitosan to interact with negatively charged bacterial membranes, ultimately causing their rupture [15]. In addition to its antibacterial activity, chitosan polycationic structure enables it to form complexes with negatively charged biomolecules such as DNA and RNA [16]. This versatility makes it highly suitable for advanced applications, including drug delivery systems [17,18]. From a production standpoint, chitin is contained in food industry by-products, primarily the exoskeletons of crustaceans. Its sustainable origin aligns with circular economy principles, reducing waste while providing a high-value biopolymer, chitosan [19,20]. According to Verified Market Research [21], the market for chitin and chitosan-derived compounds is anticipated to grow at a CAGR of 14.90 % between 2023 and 2030, reaching \$23.90 billion by that time [21]. Investigating new, alternative, and more sustainable sources is required to meet the projected growth of the world market for chitin and chitosan [10].

In recent decades, there has been a growing interest in insects as a natural source of raw materials. A growing number of industries are involved in insect farming, especially bioconverter insects such as *Hermetia illucens*, bred both for organic waste management and for the production of protein meal for animal feed [22,23]. In addition, insects provide an alternative and sustainable source of chitin and chitosan, with some advantages over crustaceans because they can be easily reared year-round and everywhere and have high fertility and reproduction rate [10]. Chitin and chitosan find many uses in various fields due to their distinctive characteristics. In the cosmetic field, chitosan is suitable for cosmetic uses in skin and hair care, because of its film-forming qualities, biocompatibility, hypoallergenicity, and antibacterial action [24,25]. It also has properties in the treatment of wounds and burns and it can be used for the production of medical plasters and reabsorbable suture materials [26–28], as well as a carrier for the controlled release of drugs [18,29,30]. To improve its performance, preparations containing chitosan are often enriched with other natural or synthetic ingredients, including clays. The physical, mechanical, and biological properties of chitosan-based films are modified by their addition [31–33]. The mechanical strength, flexibility, thermal stability, and hydrophilicity of chitosan-based materials are altered by smectite clays, such as sepiolite and montmorillonite [34]. In addition, the clays promote sustained drug release [35–37], enhance the antimicrobial activity already present in the polymer [38], and promote tissue regeneration when used in wound healing [39,40]. These properties make the chitosan-clays formulations appropriate for use in medical and cosmetic fields [41,42]. Furthermore, their ability to modulate moisture retention emphasizes their importance in developing advanced therapeutic materials [43]. The following work investigated the interaction between chitosan produced from the 3 biomasses of *H. illucens*: larvae,

pupal exuviae, and adults, with two natural smectite clays, a sepiolite (PS9) and a montmorillonite (VHS), and how they may affect the chemical and mechanical properties of insect chitosan films. Insect-derived chitosan, which offers greater sustainability than crustacean-sourced chitosan due to its absence of temporal and geographic constraints associated with traditional commercial sources, has garnered increasing interest within the global scientific community. While it has already been demonstrated to possess chemical properties comparable to those of commercial chitosan, its potential applications across diverse fields, including medical, technological, and environmental domains, now require further validation to establish it as a viable alternative or complement to crustacean-derived chitosan in industrial contexts. To the best of our knowledge, this constitutes the first work in which chitosan from *H. illucens* is complexed with clays. By exploring the technological applications of insect-derived chitosan, this work highlights its comparable and, in some cases, superior properties relative to commercial chitosan, underscoring its promise as a sustainable and effective substitute.

## 2. Materials and methods

All reagents and solvents were purchased from commercial sources and used without further purification. Commercial chitosan, glycerol, and lactic acid were purchased from Merck KGaA (Darmstadt, Hesse, Germany). *H. illucens* chitosan from larvae, pupal exuviae, and dead adults were provided by Xflies s.r.l (Potenza, Italy). Pangel S9 (PS9) was provided by TOLSA S.A. (Madrid, Spain). PS9 (pale beige powder; empirical formula:  $Mg_4Si_6O_{15}(OH)_2 \cdot 6H_2O$ ) is mainly composed of sepiolite clay and is referred as Magnesium Trisilicate in the European Pharmacopoeia [44]. Veegum HS (VHS) was purchased from Vanderbilt Minerals, LLC (Connecticut, USA). VHS (off-white powder) is a purified smectite clay which is monographed in the USP 42-NF 37 as purified bentonite [45].

### 2.1. Chitin extraction and chitosan production

For chitin extraction, raw insect biomass was frozen at  $-20\text{ }^\circ\text{C}$  and then oven-dried (18 Kw, 15 min,  $102\text{ }^\circ\text{C}$ ; MAX Microwave Dryer®, Yantai, China). The biomass was then ground using a food mill (Tom Press Italia – Mantova). The powdered samples were subjected to the chitin extraction process as reported in Hahn et al. [10]. For the removal of minerals in the powder, the samples were treated with a 0.5 M solution of formic acid ( $CH_2O_2$ ) in 1:10 w/v ratio and left under stirring for 1 h at Room Temperature (RT). The demineralized material was filtered and washed with distilled water to neutrality. The samples were then dried in an oven at  $60\text{ }^\circ\text{C}$  overnight. Protein removal involved treating the demineralized powder at a 1:10 w/v ratio with a 2 M NaOH solution at  $80\text{ }^\circ\text{C}$  for 2 h. The samples were filtered using filter paper, washed to neutral pH, and dried overnight at  $60\text{ }^\circ\text{C}$ , obtaining unbleached chitin. Finally, for obtaining bleached chitin, unbleached samples were treated for 30 to 60 min at  $90\text{ }^\circ\text{C}$  with a solution of 5 % (v/v) hydrogen peroxide ( $H_2O_2$ ) in a 1:20–30 w/v ratio, depending on the starting biomass.

According to Triunfo et al. [46], chitosan was produced by heterogeneous deacetylation of bleached and unbleached chitin from the three different biomasses of *H. illucens*, resulting in six different chitosan samples: Unbleached and Bleached Chitosan produced from Larvae (UC-L, BC-L), Pupal Exuviae (UC-PE, BC-PE), and Adults (UC-A, BC-A). Chitin samples were stirred in 12 M NaOH solution (1:20 w/v) for 4 h at  $100\text{ }^\circ\text{C}$ . The solid residue was then recovered and washed to neutrality. The deacetylated material was incubated at RT in 1 % (v/v) acetic acid for 48 h; the mixture was centrifuged for 5 min at 10,000 rpm and the supernatant was collected. To precipitate the solubilized chitosan, the solution was brought to a pH of 8 using 6 M NaOH and then incubated overnight at  $4\text{ }^\circ\text{C}$ . The precipitated chitosan was removed by centrifugation and washed till neutrality. After being freeze-dried, the obtained chitosan powder was stored at RT. The Deacetylation Degree (DD) and

Molecular weight (Mw) of the chitosan samples used for film production were assessed by potentiometric titration and by determining the intrinsic viscosity of the chitosan solutions, respectively [46].

## 2.2. Biofilm production

The solvent-casting technique [47] was used for producing all films, both those made of chitosan alone and those in which chitosan was combined with glycerol and clays. Before use, the clays used for the formulation of the films, VHS and PS9, were placed in an oven at 75–80 °C for 48 h to remove residual moisture. A suspension of chitosan was prepared at a concentration of 0.01 g/ml in 1 % lactic acid. At the same time, the clays were placed in distilled water to allow swelling and were shaken through Ultra-turrax T18 (IKA Work, Staufen, Germany). The films were produced maintaining the same solution volume/support area ratio, to ensure that the thickness of the film obtained changed as little as possible. Once poured into the chosen support, the solution was left under a fume hood at RT until complete evaporation of the solvent and formation of the film. The biofilm obtained was then removed and stored. After production, the films were initially observed at the macroscopic level, followed by optical microscopy analysis (Nikon Eclipse Inverted Light Microscope TE300/TE200 - Nikon Corporation, Tokyo, Japan), as detailed in the Supporting Information. Following several trials, the final formulation was selected, consisting of 80 % (w/w) chitosan, 10 % (w/w) clay, and 10 % (w/w) glycerol. The percentage w/w refers solely to the total weight of the added substances and not to the solution as a whole.

## 2.3. Infrared-ATR

IR spectra of the formulated films were obtained using the JASCO 6200 spectrophotometer with SPECTRA MANAGER v2 software and an Attenuated Total Reflectance (ATR) accessory (JASCO Inc., Easton, MD, USA). Measurements were carried out at wave numbers between 400 and 4000 cm<sup>-1</sup> at a resolution of 0.25 cm<sup>-1</sup>.

## 2.4. Thermal analysis

Thermogravimetric Analysis (TGA) was performed employing a METTLER TOLEDO mod (Mettler Toledo, Columbus, OH, USA), equipped with an FRS5 sensor and a precision 0.1 µg microbalance (Mettler Toledo, Columbus, OH, USA). Samples were heated at a rate of 5 °C/min in nitrogenous atmosphere. The temperature ranges employed were 30–950 °C.

## 2.5. X-ray diffraction

X-Ray Diffraction (XRD) analysis of the chitosan and clay powders was performed using a PANalytical X'Pert Pro diffractometer (Malvern Panalytical, UK), equipped with an X'Celerator solid-state detector and a rotating sample holder. The diffraction patterns were recorded using randomly oriented mounts with CuKα radiation, operating at 45 kV and 40 mA, over a range of 3–50° 2θ (step size of 0.008° 2θ, with a scan time of 9.73 s per step). The same conditions were applied for the analysis of the resulting films.

## 2.6. Wettability test

Membrane wettability was assessed by the sessile drop method, according to the European Pharmacopoeia [48]. An instrument consisting of a dispensing syringe, a surface on which to fix the sample, a microscope camera with 40× magnification (PixelINK PL-A661, 1.3 Megapixel monochrome FireWire IEEE 1394, Ottawa, ON, Canada), and a white light source were used to carry out the assay. The syringe, containing distilled water inside, was used to deposit 5-µL drops onto the film surface. The wettability of the films was assessed exclusively at the

moment the drop made contact with the analyzed film. Once the image was acquired, the amplitude of the tangent angle to the drop was determined manually using a protractor. The wetting angle was determined as the angle between the tangent to the droplet at the contact point and the surface of the film.

## 2.7. Film thickness

A caliper micrometer was used to measure the thickness of the films (Digimatic Caliper No. 99MAD027M3, Mytutoyo Manufacturing Co. Ltd., Japan). For the measurements, the films were cut into squares with a side length of 30 mm. For each film type, the thickness of all 4 corners of the square was measured, repeating the measurements in triplicate [49].

## 2.8. Mechanical characterization

### 2.8.1. Tensile strength

The Tensile Strength (TS) of the films was measured using a TX.AT plus Texture Analyzer (Stable Micro Systems, UK), equipped with a 5 kg load cell and an SMS P/5S probe. Homogeneous films of 30 mm by 30 mm were prepared for this test. These films were placed on a platform and secured with the corresponding holder for the puncture test, leaving a circular gap of 5 mm radius at the center through which the probe would pass. During the measurement, the probe attempted to penetrate the film at a speed of 1 mm/s until the film ruptured. Elongation At Break (EAB) and TS were recorded at the point of breakage. Each film type was tested five times. The TS and EAB were calculated according to Eq. (1) and Eq. (2), respectively:

$$\text{Tensile Strength (MPa)} = \frac{F_{\max}}{A} \quad (1)$$

where  $F_{\max}$  (N) is the force applied immediately before rupture, and  $A$  (mm<sup>2</sup>) represents the contact area between the probe and the sample, calculated based on the measurements of the thickness and width of the sections [50].

$$\text{Elongation at Break (\%)} = \left( \frac{\sqrt{a'^2 + b^2 + r} - a}{a} \right) * 100 \quad (2)$$

where  $a'$  (mm) is the distance from the edge of the holder gap to the center of the probe,  $a$  (mm) is the radius of the holder gap (if the platform is properly aligned,  $a' = a$ ),  $b$  (mm) is the distance traveled by the film until breakage, and  $r$  (mm) is the radius of the probe.

### 2.8.2. Adhesion test

The aforementioned Texture Analyzer (TX.AT plus Texture Analyzer, Stable Micro Systems, UK), equipped with a 5 kg load cell and a P/10 probe, was also used to measure the adhesive capacity of the films. Homogeneous films were cut into circular fragments with a diameter of 10 mm using a metal punch and were attached to the P/10 probe using double-sided tape. The adhesion test was carried out following part of the methodology published by Alaei et al. [51]. The analysis was conducted in compression mode, with a test speed of 0.1 mm/s, a post-test speed of 10 mm/s, and a hold time of 10 s. Each film was brought into contact with an 8 % (w/w) gelatin substrate at RT. The adhesion force, defined as the maximum negative force recorded, was used to express the results. Five replicates were performed for each sample to ensure accuracy.

## 2.9. Statistical analysis

All measurements were performed in replicate and data were expressed as average ± standard deviation. Data were analyzed by one-way Anova and Tuckey *post-hoc* test. Statistical analyses were performed

using a GraphPad Prism version 8.4.2 for Windows (GraphPad Software, San Diego, California USA).

### 3. Results and discussion

#### 3.1. Chitosan samples

Starting from the 3 biomasses of *H. illucens*, six types of chitin samples were obtained and subjected to deacetylation, resulting in six different chitosan samples: Unbleached and Bleached Chitosan produced from Larvae (UC-L, BC-L), Pupal Exuviae (UC-PE, BC-PE) and Adults (UC-A, BC-A), respectively. The chitosan samples obtained differ in some characteristics, such as their crystalline structure, Molecular weight (Mw), and Degree of Deacetylation (DD) [46]. The characteristics of each sample are shown in Table 1.

#### 3.2. Chitosan-clay films production

The solvent casting technique was used to prepare the biofilms [47]. For Chitosan-Clay Nanocomposite Films (C-C NFs) once all the components, consisting of 80 % chitosan (w/w), 10 % clay (w/w), and 10 % glycerol (w/w), were combined, the suspension was transferred to the holder and dried under a fume hood. As shown in Fig. 1, twelve different films were produced using two different chitosan samples derived from the three biomasses of *H. illucens* (Bleached and Unbleached Chitosan from Larvae, Pupal Exuviae, and Adults) and two different natural clays, PS9 and VHS.

The obtained films were examined under a light microscope at 4× magnification. Given the compactness of their particles and their inherent opacity [52,53], most clays do not allow visible light to pass through. Thus, the dark areas in the images indicate the distribution of phyllosilicates within the preparation. In contrast, chitosan films are transparent and permit light to pass through [54], making the lighter areas in the images representative of the polymer network formed by chitosan. The images demonstrate a homogeneous distribution of both components, with a well-organized polymer network visible for both types of clay. Notably, bleached (BC) samples exhibit a more uniform particle distribution and a denser polymer network compared to the unbleached (UC) ones. In films containing PS9, areas with a higher concentration of clay are particularly evident, especially in the UC samples, highlighting the relationship between biofilm morphology and the type of chitosan utilized. For the films containing VHS, the distribution appears less homogeneous across different regions of the film, although no distinct separation between clay-rich and chitosan-rich areas is observed (Fig. 2). This could be due to the different nature of the two clays. Indeed, montmorillonite, with its layered structure composed of silica and aluminum sheets, allows for the intercalation of polymers like chitosan within its interlaminal spaces, leading to a more homogeneous composite structure [55]. In contrast, sepiolite, due to its fibrous and porous nature, does not facilitate intercalation in the same way. Instead, its interaction with polymers tends to form a network that

**Table 1**

Degree of Deacetylation (DD%) and Molecular weight (Mw) of chitosan from *H. illucens* used for biofilm production. The table shows the DD and Mw values for all samples: Unbleached Chitosan from Larvae (UC-L), Bleached Chitosan from Larvae (BC-L), Unbleached Chitosan from Pupal Exuviae (UC-PE), Bleached Chitosan from Pupal Exuviae (BC-PE), Unbleached Chitosan from Adults (UC-A), Bleached Chitosan from Adults (BC-A).

Chitosan sample	DD%	Mw
UC-L	85–90 %	100–120 kDa
BC-L	80–85 %	48–60 kDa
UC-PE	80 %	180–220 kDa
BC-PE	80–85 %	48–60 kDa
UC-A	80 %	180–220 kDa
BC-A	85–90 %	48–60 kDa

results in a more heterogeneous distribution of the components [56]. This fibrous structure likely contributes to the less uniform dispersion of sepiolite within the polymer matrix [57–59].

#### 3.3. ATR-FTIR

Spectra resulting from ATR-FTIR analysis of chitosan-clays films and pure clays are shown in Fig. 3. In all film spectra, the characteristic signals of chitosan can be clearly observed. Firstly, a broad band appears between 2700 and 3400  $\text{cm}^{-1}$ , which corresponds to the CH stretching vibrations (between 2800 and 2900  $\text{cm}^{-1}$ ) and the O—H and N—H stretching vibrations (between 3100 and 3300  $\text{cm}^{-1}$ ) [56]. Additionally, an intense band between 900 and 1100  $\text{cm}^{-1}$ , characteristic of the  $\beta$ -glycosidic linkages, is visible [59]. The region between 1200 and 1700  $\text{cm}^{-1}$  is associated with amide groups. Within this region, a signal can be observed around 1600  $\text{cm}^{-1}$ , corresponding to N—H bending in secondary amides, and another near 1700  $\text{cm}^{-1}$  related to C=O stretching in primary amides [46,61]. Some differences compared to the spectra reported by Triunfo et al. [46], which are derived from powdered chitosan extracted from *H. illucens*, are found in the amide region, where the primary amide band appears at 1655  $\text{cm}^{-1}$  and the secondary amide band at 1590  $\text{cm}^{-1}$ . The protonation of amino groups, which overlap with some amide bands, may be the cause of this variance. The polymer intercalating between the clay layers is another possible reason for the shift to lower wavenumbers [60]. Characteristic bands of sepiolite (PS9) and montmorillonite (VHS) are also discernible in the clay spectra. In the VHS spectrum, there is an identifiable band above 3500  $\text{cm}^{-1}$ , which is associated with the OH groups of octahedral layers, notably Al—OH—Al, Al—OH—Mg, and Mg—OH—Mg vibrations. Additionally, a major band at 1000  $\text{cm}^{-1}$  is present, which is attributed to in-plane stretching vibrations of the silicate layers (Si—O—Si). This broad band overlaps with vibrations from the out-of-plane Si—O—Si stretching (above 1000  $\text{cm}^{-1}$ ) and also with another signal related to Si—O—Al bending vibrations [62]. The PS9 spectrum also exhibits a prominent band at 1000  $\text{cm}^{-1}$ , linked to Si—O stretching vibrations, as well as a characteristic band for fibrous clays associated with Si—O—Si linkages between alternating fibers (due to oxygen inversion in the tetrahedra) at 1200  $\text{cm}^{-1}$ , which overlaps with the previous band [63]. Finally, the signal observed around 1000  $\text{cm}^{-1}$  in the chitosan-clay spectra results from the superimposition of the characteristic bands of each component, leading to more intense signals than those found in the spectra of pure chitosan as reported by Triunfo et al. [46,60].

#### 3.4. Thermal analysis

For Thermogravimetric Analysis (TGA), approximately 10 mg of the biofilms were finely minced until very small pieces were obtained. TGA and DTG curves of analyzed films are shown in Fig. 4. The weight loss observed at various temperature ranges is summarized in Table 2. The table highlights the distinct thermal degradation behavior of each sample. Weight loss peaks observed between 35 and 150 °C can be attributed to residual moisture loss, while those between 150 and 250 °C are associated with the thermal degradation of glycerol in the samples containing VHS and PS9 clays, as well as the evaporation of the trapped water [64,65]. At higher temperatures, the peaks observed in the range 250–450 °C and in the range 450–950 °C represent the degradation of the chitosan polymer network [66–68].

BC-L, UC-L, BC-PE, UC-PE, BC-A, and UC-A samples, which do not contain glycerol or any type of clay, show differences in their thermal degradation behavior. The BC-L sample shows a total weight loss of 73.43 %, while UC-L exhibits a slightly higher value of 77.23 %, indicating that BC-L is more thermally stable. BC-PE, on the other hand, has the lowest total weight loss among chitosan films, at 69.69 %, suggesting better resistance to thermal degradation than its unbleached counterpart and other samples. Similarly, for adult biomass, bleached chitosan demonstrates better resistance to thermal degradation, with the BC-A

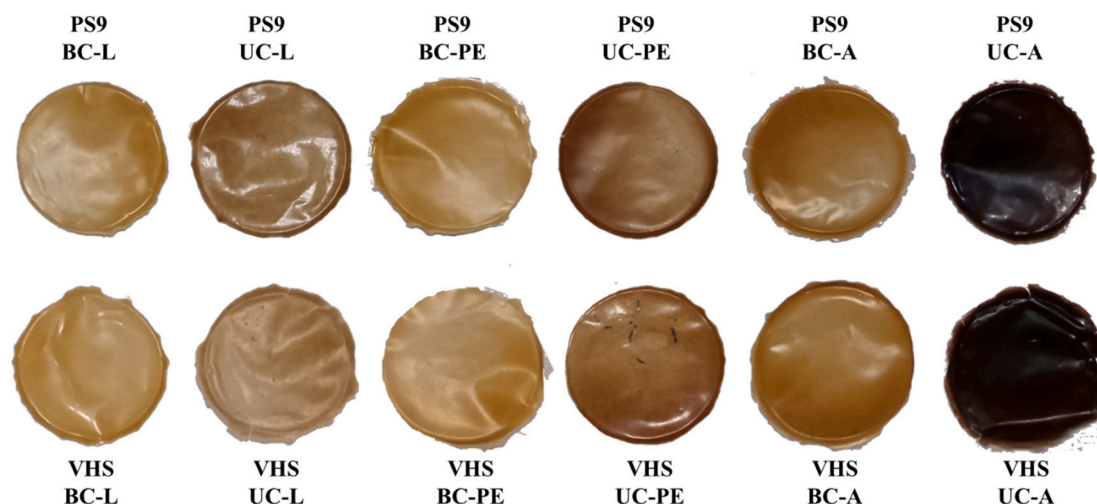


**Fig. 1.** Chitosan-Clay Nanocomposite Films (C-C NFs). C-C NFs were produced from Bleached (BC) and Unbleached Chitosan (UC) from Larvae (L), Pupal Exuviae (PE), and Adults (A) of *H. illucens* and combined with two natural clays, PS9 and VHS.

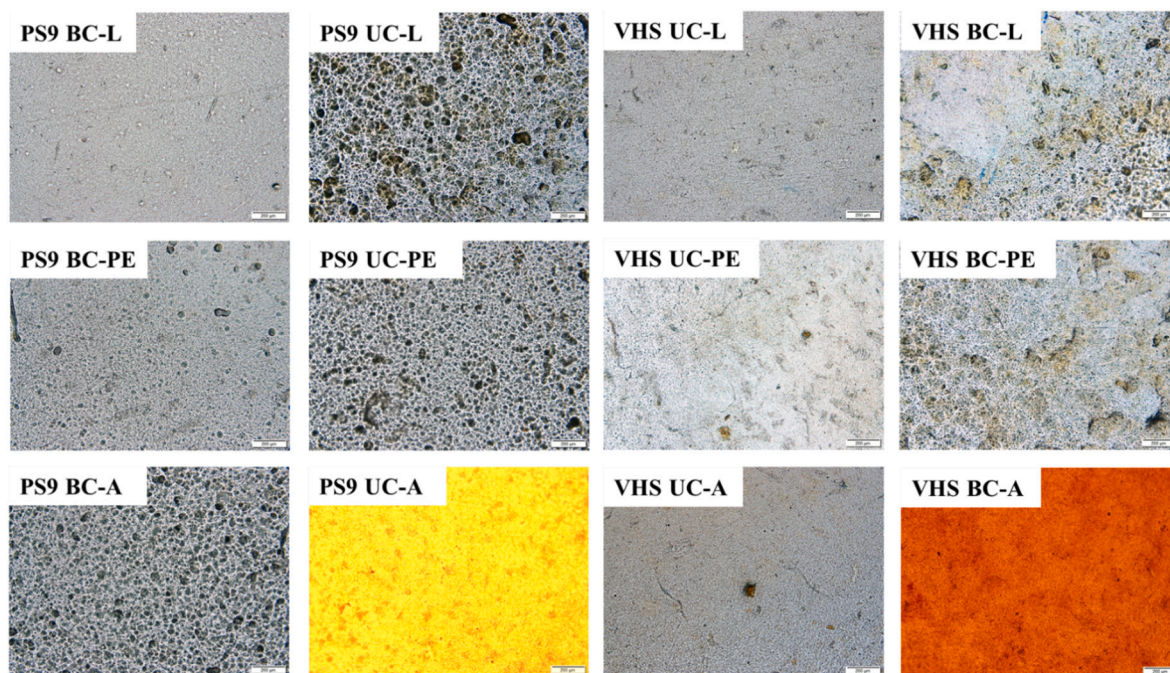


**Fig. 2.** Optical microscope images of C-C NFs. C-C NFs were produced with two different clays (PS9 and VHS) and six different chitosans from *H. illucens* biomasses. The observation offers a preliminary evaluation of the homogeneity of the films. The lighter areas represent regions where the chitosan allows light to pass through, while the darker areas indicate the presence of the clay, which is opaque. A more uniform distribution of light and dark areas suggests better dispersion of the clay within the polymer matrix, leading to a more homogeneous film.

film showing a lower weight loss than UC-A. For all films composed exclusively of chitosan, BC samples demonstrated better resistance to thermal degradation compared to UC ones. This indicates that the bleaching process can improve the thermal stability of chitosan-based films. Among the different biomass sources, PE-derived films exhibited the greatest resistance to thermal treatment, with the BC-PE sample showing the least overall weight loss.

In comparison, the samples containing glycerol and clays (VHS and PS9) display different thermal behaviors. In the 150–250 °C range, decomposition of glycerol and trapped water contributes significantly to the observed weight loss, so these losses do not reflect the stability of the chitosan-clay matrix itself. To evaluate the influence of clays addition on the biofilm, we must focus on the weight loss that occurs at higher

temperatures, mainly above 250 °C, where the influence of glycerol is no longer a determining factor. Starting from the PS9 samples, the weight loss in the 250–450 °C range for PS9 BC-L is 35.21 %. Comparing it with sample BC-L, which is composed exclusively of chitosan and does not contain clays, a weight reduction of 47.59 % is observed. BC-PE shows a similar trend, losing 47.27 % of its weight, while when combined with clay it shows a smaller weight loss of 34.43 % within the same range. This trend is also confirmed by the PS9 BC-A sample, which reports a loss of 36.11 % compared to the 48.48 % by weight lost by its counterpart without clay. Similarly, if we consider VHS-containing films, the improvement in thermal stability is similarly evident. VHS BC-L shows a weight loss of 35.58 % in the range of 250–450 °C, lower than the film consisting of chitosan alone, but slightly higher than the film containing

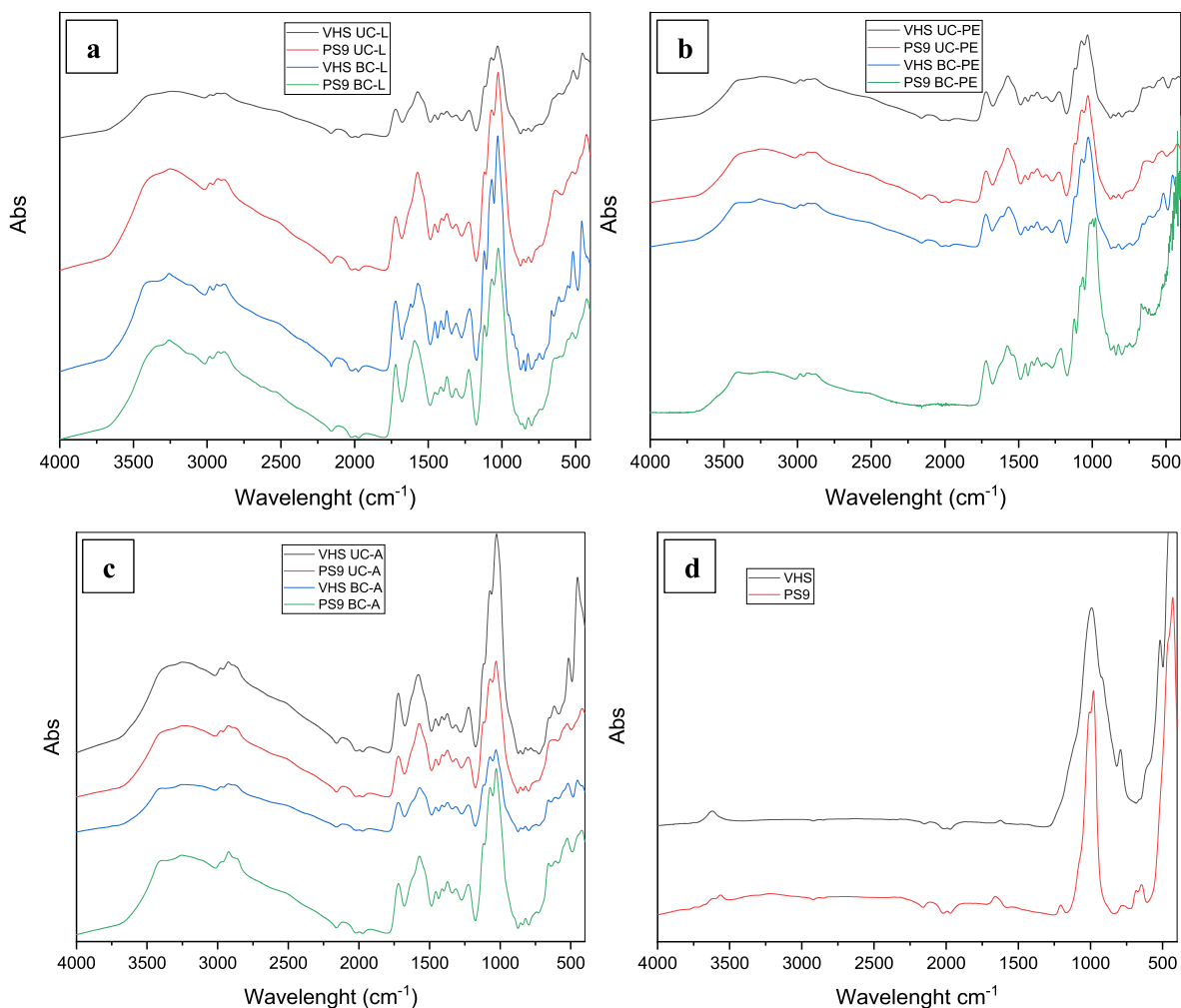


**Fig. 3.** ATR-FTIR spectra of C-C NFs derived from the various biomasses of *H. illucens*: Larvae (a), Pupal Exuviae (b), and Adults (c) and of the two clays used in the production of the biofilms (d).

PS9. This trend is also found in other biomasses. VHS BC-PE shows a weight loss of 35.24 %, while VHS BC-A records a weight loss of 36.6 %. Upon comparing the effects obtained with the two clays, it can be stated that PS9 films had slightly better thermal stability. However, the addition of both types of clays resulted in an improvement in the thermal stability of the formulation compared to the non-clay films, indicating that both types of clays play a role in stabilizing the polymer network during thermal degradation.

Further comparisons can also be made between the different biomass types. For the PS9 films, PS9 BC-L (35.21 %) and PS9 BC-A (36.11 %) show slightly higher weight losses compared to PS9 BC-PE (34.43 %). A similar trend is seen with the VHS samples, where VHS BC-L (35.58 %) and VHS BC-A (36.6 %) lose more weight than VHS BC-PE (35.24 %). This suggests that, regardless of the type of clay used, the films containing PE biomass exhibit a somewhat denser and more thermally stable polymer network than the other biomass types. The sensitivity of biopolymers to heat is one of their primary problems, which restricts the use of both conventional processing techniques like extrusion or molding as well as drying and sterilizing procedures. According to the findings of our experiments, chitosan films show great thermal stability and do not significantly degrade or change structurally when subjected to high temperatures, such those needed for sterilizing procedures. Compared to other biopolymers, such collagen or alginate, which are frequently heat-sensitive and prone to denaturation or deterioration under comparable circumstances, chitosan thermal durability makes it an attractive biopolymer for biomedical applications requiring asepsis

[69].

### 3.5. X-ray diffraction

The diffractograms for all the studied samples are shown in [Figs. 5 and 6](#). The diffractograms of films made exclusively from chitosan (K, BC-L, UC-L, BC-PE, UC-PE, BC-A, UC-A) are reported in [Fig. 5a](#), and display two prominent reflections around  $6^\circ$  and  $20^\circ$   $2\theta$ , with the first being the most intense. The peaks obtained from the analysis of the chitosan-only films differ from those exhibiting chitosan from *H. illucens* powder ([Fig. 5b](#)) and from those obtained from insect and crustacean chitosan in other studies where the reflection peaks typically appear at  $10^\circ$  and  $20^\circ$   $2\theta$  [10,70] with the latter peak more intense than the first one. The peak present at  $10^\circ$   $2\theta$  is associated with the hydrated crystalline polymorph, while the one at  $20^\circ$   $2\theta$  corresponds to the regular crystal network of chitosan [71]. During the film preparation process, chitosan is dissolved in an aqueous solution and air-dried. This process does not ensure complete dehydration and, consequently, a more intense first peak is present in the diffractograms of the films, indicating a higher percentage of hydrated crystals. Instead, as in the case of powdered chitosan, where the non-hydrated crystalline form predominates, the reflection at  $20^\circ$   $2\theta$  is more intense. Notably, the first peak is attributed to the formation of intramolecular hydrogen bonds; increased hydration of the crystalline structure allows water molecules to intercalate, leading to greater separation between the polymer fibers [72], causing a shift of the peak towards lower angles, in accordance

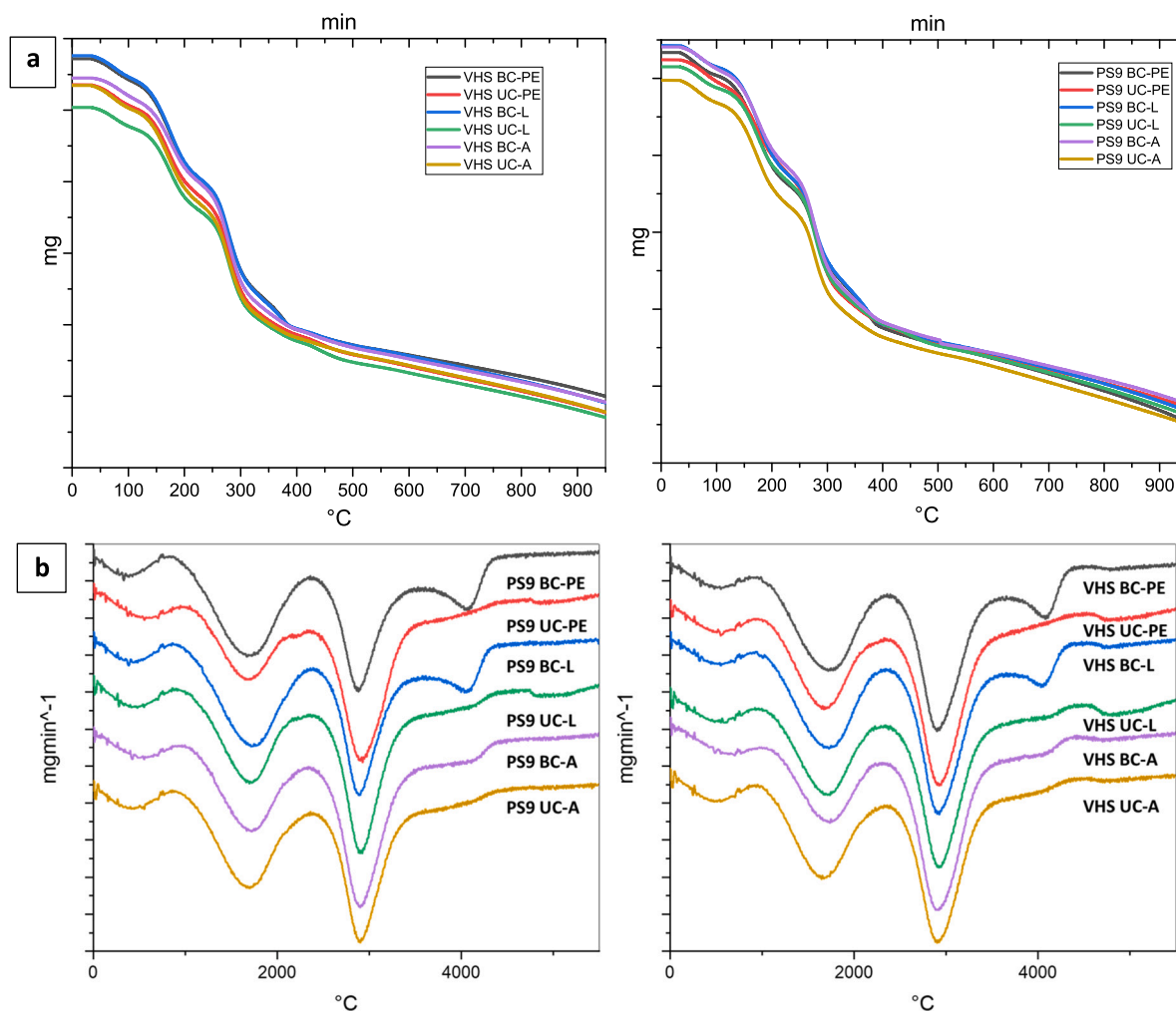


Fig. 4. TGA (a) and DTG (b) curves for C-C NFs samples.

with Bragg's law. This explains why the reflection corresponding to the hydrated polymorph occurs at angles below  $10^\circ 2\theta$ .

Furthermore, in the case of K films, the first peak is less intense and located at a higher  $2\theta$  angle, suggesting that this type of chitosan absorbs less water compared to *H. illucens* chitosan. For film production, it is essential for water molecules to be incorporated into the crystalline structure, as this is how chitosan exhibits its chemical and biological properties [73]. In this regard, *H. illucens* chitosan could be more advantageous than crustacean-derived chitosan, where the non-hydrated crystal structure peak is more intense.

In the diffractograms of powdered chitosan (Fig. 5b), the most intense peaks, associated with higher crystallinity, are observed for decolorized chitosan, consistent with trends reported in the literature [46]. However, the opposite seems to occur in films made solely from chitosan (Fig. 5a). This discrepancy may arise from the fact that decolorized chitosan, being more ordered, is more difficult to disrupt during film preparation, preventing recrystallization that would otherwise occur in unbleached chitosan films, where water molecules intercalate into the polymer, leading to higher peaks associated with the hydrated crystalline structure [71].

Fig. 6 shows diffractograms of the films made from the different types of chitosan and diffractograms of all individual components for better comparison. For the films containing clay, characteristic peaks of each clay are visible. The diffractogram of VHS shows a primary peak at  $7.5^\circ 2\theta$ , corresponding to an interlayer spacing of 12 Å. Additionally, peaks appear around  $20^\circ$  and  $22^\circ 2\theta$  [62], which are visible in the

spectra shown in Fig. 6. Due to the film treatment, the diffractograms of the clays should be interpreted as those of oriented aggregates. Thus, the first peak in the VHS-containing films corresponds to the  $7.5^\circ 2\theta$  reflection of powdered clay, though it shifts towards  $5^\circ 2\theta$ , indicating an increase in interlayer spacing typical of smectites. This shift could be due to the intercalation of chitosan into the interlayer space of montmorillonite, justifying the use of the term "nanocomposite" to describe the polymer-clay interaction in these films [74]. In particular, the resulting interlayer space after the inclusion of the polymer, corresponded to the effective inclusion of two polymer chains into the clay interlayer [55].

The diffractogram of powdered PS9 exhibits all the characteristic reflections of this mineral, consistent with existing literature [63]. The most intense reflection corresponds to the peak at  $7^\circ 2\theta$ , indicating a spacing of 12.15 Å. In the case of sepiolite, this interlayer spacing remains unchanged, as it is fixed due to the continuous spatial arrangement of the tetrahedral layers [56]. In fact, the zeolitic channels do not change in dimension, even in the presence of water molecules or other compounds [75], making this a key difference compared to VHS. Consequently, in the diffractogram of PS9 films, this reflection remains unaltered, appearing in the same position.

Additionally, a second peak appears at  $9^\circ 2\theta$ , corresponding to the presence of impurities, specifically the mineral phase muscovite, as reported in oriented aggregate analyses of PS9 sepiolite in the literature [63]. The films made with BC and PS9 show the characteristic first peak of the clay, but also a small peak around  $7^\circ 2\theta$  (associated with hydrated chitosan), suggesting that part of the polymer is not interacting with the

**Table 2**

Weight Loss (WL%) of C-C NFs at different temperature ranges (35–150 °C, 150–250 °C, 250–450 °C, and 450–950 °C) as measured by TGA.

Sample	WL% 35–150 °C	WL% 150–250 °C	WL% 250–450 °C	WL% 450–950 °C	TOTAL WL%
BC-L	8.67	–	47.59	17.17	73.43
UC-L	7.84	–	50.38	19.01	77.23
BC-PE	7.94	–	47.27	14.48	69.69
UC-PE	6.68	–	48.88	17.54	73.1
BC-A	7.15	–	48.48	14.67	70.3
UC-A	10.01	–	46.64	18.79	75.44
VHS BC-L	11.16	21.69	35.58	16.08	84.51
VHS UC-L	10.62	21.32	36.13	18.26	86.33
VHS BC-PE	11.09	21.91	35.24	14.54	82.78
VHS UC-PE	11.04	21.39	35.68	17.73	85.84
VHS BC-A	10.02	20.44	36.6	16.39	83.45
VHS UC-A	12.14	22.22	33.93	17.41	85.7
PS9 BC-L	10.8	22.97	35.21	18.83	87.81
PS9 UC-L	10.47	21.61	35.65	20.52	88.25
PS9 BC-PE	12.25	22.61	34.43	21	90.29
PS9 UC-PE	10.92	20.96	36.42	18.11	86.41
PS9 BC-A	10.75	21.59	36.11	17.58	86.03
PS9 UC-A	12.21	23.46	33.72	20.68	90.07

clay. Moreover, the diffractograms of BC films with VHS show lower and slightly shifted peaks, indicating that the interaction with the polymer is weaker compared to UC films.

In the diffractograms of UC, especially those from PE and A, the small peak at  $7^\circ 2\theta$  (related to hydrated chitosan crystals) is absent, suggesting that the presence of clay particles hinders the formation of the hydrated chitosan polymorph, indicating stronger interaction between the two components. Similarly, it is challenging to detect chitosan in the VHS-containing films because the reflections of VHS and chitosan overlap. However, the fact that the VHS reflection (around  $8^\circ 2\theta$ ) is not visible in the film diffractograms suggests a shift towards lower angles, indicating an increase in basal spacing. This shift could be attributed to the intercalation of chitosan into the interlayer space, signifying a physical interaction between the polymer and the clay [71].

### 3.6. Film thickness

Film thickness is a critical parameter in the characterization of thin films, because it directly influences various properties, such as mechanical strength, barrier performance, optical characteristics, and overall functionality of the material [76,77]. Quantitative analysis of biofilm thickness is also crucial for ensuring homogeneity, which enhances the reliability and quality of experimental outcomes in biofilm research [78].

From the results obtained, reported in the Supporting Information section, it is clear that the thickest film without additives is BC-L, with an average thickness around 0.082 mm, while the thinnest film is UC-L, with an average thickness close to 0.053 mm. These differences suggest that the specific chitosan types (K, PE, L, and A) play a role in determining the overall film thickness. Films containing K tend to have slightly lower thickness values, whereas those incorporating PE and L show greater variability.

When comparing BC with UC, it seems that the bleaching process generally leads to the production of thicker films. Across the different

biomasses (L, PE, A), the BC films consistently show greater thickness than their UC counterparts. This indicates that the bleaching process, which removes pigments and other impurities, may contribute to structural changes in the chitosan matrix that lead to produce thicker films. In contrast, the addition of clays does not show a clear trend of increasing or decreasing thickness.

### 3.7. Wettability test

Analyzing the contact angle data provides insights into the hydrophilicity or hydrophobicity of the chitosan films. Contact angles greater than  $90^\circ$  indicate hydrophobic properties, whereas angles below  $90^\circ$  indicate a more hydrophilic character [79]. Fig. 7 shows the results obtained from the wettability test. From the values provided, it is possible to assess how the addition of clays (VHS and PS9) as well as the different types of chitosan used (K, L, PE, and A) influence the surface properties of the films.

The film made from pure commercial chitosan (K) showed a contact angle of approximately  $67.5^\circ$ , which indicates a relatively hydrophilic surface. However, upon the addition of VHS and PS9, the contact angles increased to  $71.9^\circ$  and  $68.7^\circ$ , respectively. Although both clays made the chitosan films more hydrophobic, VHS provides a higher degree of hydrophobicity than PS9 in these formulations.

In the films obtained from larvae (L), the addition of VHS and PS9 significantly increased the contact angles compared to the film without clay (BC-L and UC-L). The contact angle for BC-L was  $69.6^\circ$ , indicating a moderately hydrophilic nature. When VHS and PS9 were added, the angles increased to  $84.5^\circ$  and  $81.75^\circ$ , respectively. For the UC-L sample, the contact angle was  $60.5^\circ$  and, with the addition of the two clays, the value increased to  $85.8^\circ$  for VHS and  $83.1^\circ$  for PS9.

The PE films demonstrated a similar pattern. The pure PE films (BC-PE and UC-PE) had a contact angle of  $68.2^\circ$  and  $62.5^\circ$  respectively, indicating a hydrophilic surface. Adding VHS led to a significant increase in the contact angle, reaching  $84^\circ$  for VHS BC-PE and  $81.7^\circ$  for VHS UC-PE. The addition of PS9 led to an even higher value for PS9 BC-PE, with the contact angle increasing to  $90.5^\circ$ , while a slightly lower angle of  $81.5^\circ$  was observed for PS9 UC-PE.

When evaluating films derived from adult chitosan (A), the trend was again similar. The BC-A and UC-A films, without clay, had a contact angle of  $72.6^\circ$  and  $58.8^\circ$  respectively, reflecting a relatively hydrophilic character. The introduction of VHS resulted in a substantial increase to  $80.8^\circ$  for VHS BC-A, and an even more pronounced increase to  $92.2^\circ$  for VHS UC-A, indicating a shift towards a hydrophobic surface. Adult films containing PS9 also showed an increase in hydrophobicity, with contact angles of  $89.7^\circ$  (PS9 BD-A) and  $88.3^\circ$  (PS9 UC-A), though the change was less pronounced compared to the addition of VHS.

For all samples the contact angle increases in formulations containing clay, indicating increased hydrophobicity. This effect is noteworthy considering that these films also contain glycerol, a plasticizer that typically reduces contact angle by increasing hydrophilicity [80]. Both VHS and PS9 clays increased the hydrophobicity of the chitosan films, but VHS generally produced higher contact angles than PS9 across all chitosan sources. The observed increase in hydrophobicity following the addition of inorganic excipients is consistent with findings previously reported in the literature [79,81]. This increase may be due to the interaction between chitosan and clay in the nanocomposite films, which reduces the number of available hydrophilic groups in chitosan that can interact with water [79,81]. The hydrophobicity of the films varied depending on the source of chitosan used. Films derived from K exhibited lower contact angles compared to films derived from L, PE, and A and thus lower hydrophobicity.

While greater hydrophilicity is generally advantageous for applications involving skin or mucosal contact, excessive hydrophilicity can sometimes be counterproductive. For instance, in formulations intended for use on wounds with exudate or on wet skin, a highly hydrophilic film may dissolve too quickly, potentially limiting its effectiveness and

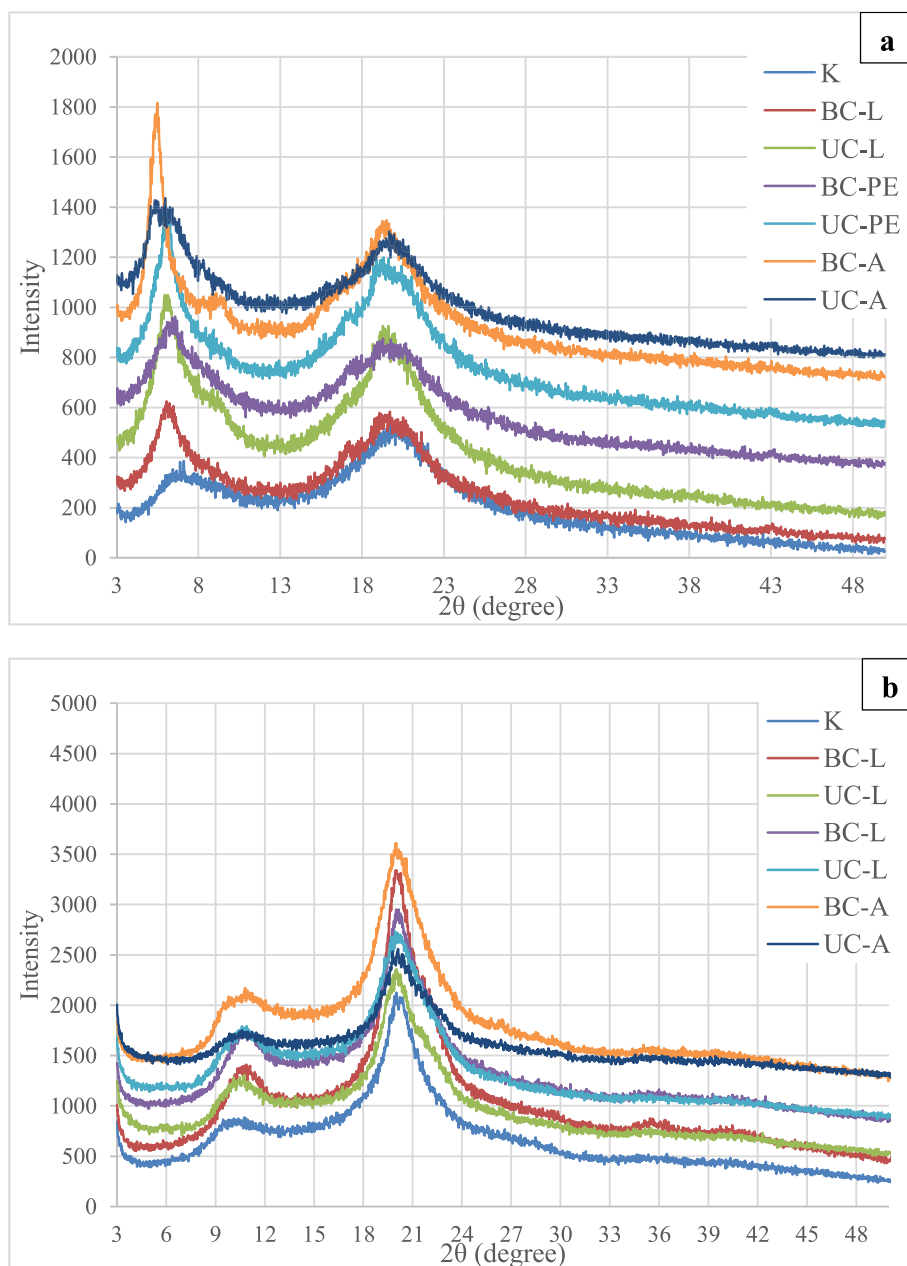


Fig. 5. X-ray diffractograms of films composed solely of chitosan (a) and of chitosan powders analyzed as utilized (b).

altering the release profile of active substances, if present [82,83].

### 3.8. Mechanical characterization

#### 3.8.1. Tensile strength

The TS test provides information on the mechanical properties of the chitosan-based films and indicates how much force a material can withstand before breaking (Fig. 8). The pure K film exhibits a relatively high tensile strength, reaching a resistance of 1.09 MPa. In contrast, the A-derived chitosan exhibits a lower tensile strength, with values for BC-A and UC-A being 0.46 MPa and 0.63 MPa, respectively. PE-derived chitosan shows tensile strength values comparable to A films. UC-PE reaches 0.85 MPa, which is higher than the 0.58 MPa of BC-PE, but in both cases below the values observed in K. On the other hand, L chitosan shows an interesting pattern. While BC-L has a tensile strength of 0.59 MPa, similar to the BC forms of other chitosans, the UC-L variant reaches the highest tensile strength of all sources at 1.21 MPa. This suggests that

UC-L offers good mechanical integrity, even outperforming K. UC consistently leads to better resistance compared to BC, for all formulations tested. Although UC chitosan has lower crystallinity than BC, this seems to favor the mechanical properties in the context of TS, suggesting that the molecular weight or the amorphous regions in UC chitosan allow for better flexibility and stress distribution. Bleaching process could reduce the mechanical performance of the films, potentially due to structural alterations or reduced molecular weight. The XRD data further corroborates this, as the characteristic chitosan peaks are still visible in the diffractograms of BC films containing clay, suggesting insufficient intercalation of the clay into the chitosan matrix or a lower degree of interaction (Fig. 6). Interestingly, UC films with PS9 perform relatively better than those with VHS. This suggests that PS9, despite being less effective in the BC films, may form a more favorable interaction with UC. It is possible that the molecular structure and higher molecular weight of UC facilitate better dispersion or bonding with PS9 particles. The improved dispersion of PS9 in UC films could explain the

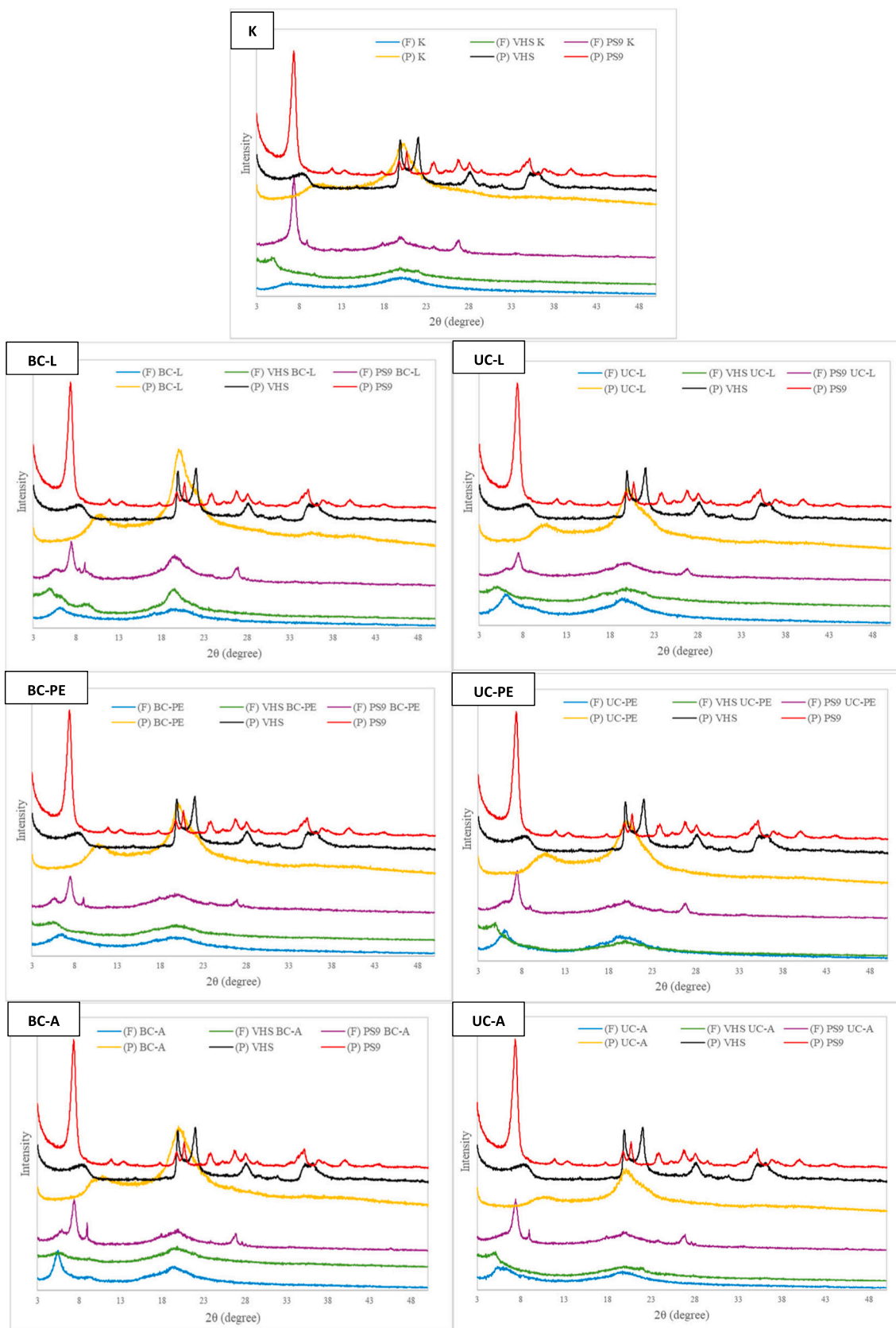


**Fig. 6.** X-ray diffractograms of C-C NFs and their individual components. The diffractograms provide insights into the crystalline structures of the films, highlighting differences in crystallinity and phase behavior among the chitosan types and their respective components. The red, black, and yellow lines correspond to the substances used for the production of the films analyzed as-is, specifically PS9, VHS, and chitosan from the various biomasses, respectively. The blue, green, and purple lines correspond to the biofilms, specifically chitosan-only films from the analyzed biomass (K, L, PE, A), films with VHS, and films with PS9, respectively. (For interpretation of the references to color in this figure legend, the reader is referred to the web version of this article.)

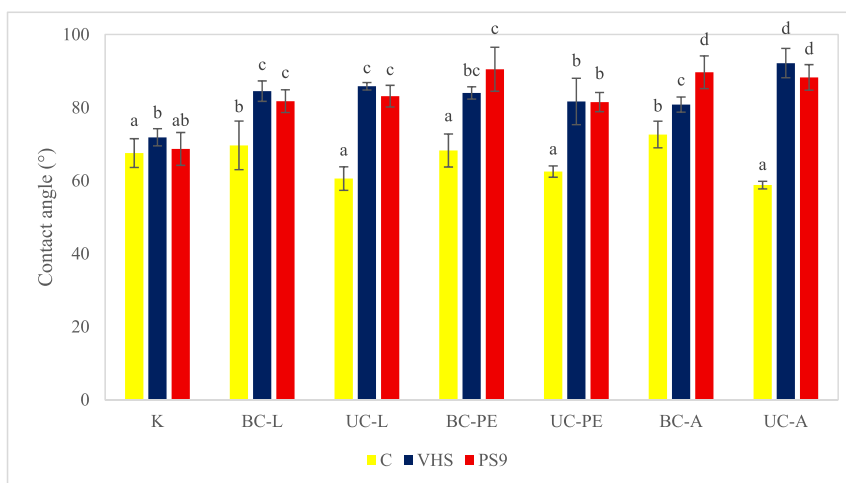


**Fig. 7.** Contact angle results expressed in degree (°) for each of the film formulations (mean  $\pm$  s.d.;  $n = 5$ ). The film samples are grouped into seven groups according to the type of chitosan used for film production (K, BC-L, UC-L, BC-PE, UC-PE, BC-A, UC-A). Within each group, the yellow bar (C) corresponds to the film produced with only chitosan, the blue bar (VHS) to the films containing montmorillonite, and the red bar (PS9) to those containing sepiolite. The statistical analysis presented in the graph was conducted separately for each biomass (K, L, PE, A). For the analysis comparing the results across all samples, please refer to the “Supporting Information” section. (For interpretation of the references to color in this figure legend, the reader is referred to the web version of this article.)

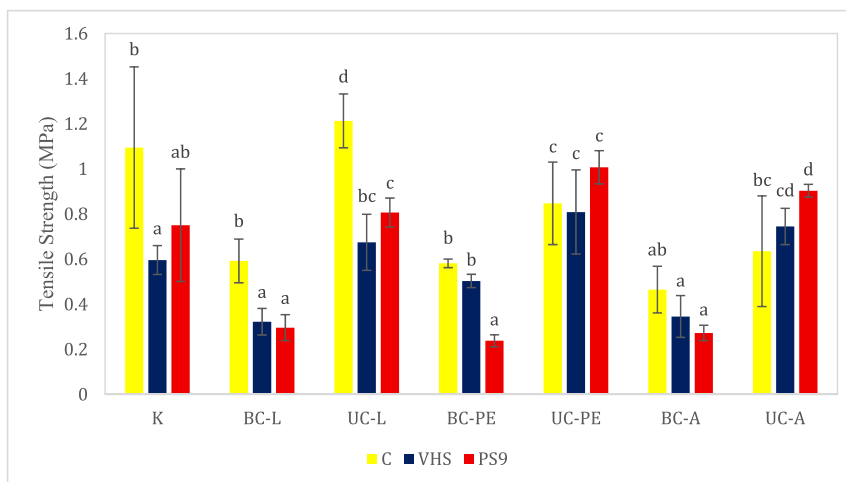


**Fig. 8.** TS results expressed in MPa for each of the film formulations (mean  $\pm$  s.d.;  $n = 5$ ). The film samples are grouped into seven groups according to the type of chitosan used for film production (K, BC-L, UC-L, BC-PE, UC-PE, BC-A, UC-A). Within each group, the yellow bar (C) corresponds to the film produced with only chitosan, the blue bar (VHS) to the films containing montmorillonite, and the red bar (PS9) to those containing sepiolite. The statistical analysis presented in the graph was conducted separately for each biomass (K, L, PE, A). For the analysis comparing the results across all samples, please refer to the “Supporting Information” section. (For interpretation of the references to color in this figure legend, the reader is referred to the web version of this article.)

enhanced puncture resistance, as homogeneously dispersed clay particles within the polymer matrix are known to provide better stress transfer during mechanical loading [74]. The superior mechanical properties of UC could offer an advantage since the decolorization step would not be required in the chitosan production process, thus saving both time and resources.

Addition of VHS and PS9 clays generally reduced the tensile strength of the films, except for UC-A and UC-PE samples, where an increase in strength was found upon addition of both clays. With these types of chitosan, clay-containing films appear to exhibit improved TS probably due to a homogeneous dispersion of rigid clay particles within the polymer matrix, forming strong ionic and interfacial adhesion bonds [84]. For UC-PE and A, a stronger clay-polymer interaction is also evident in the X-ray analysis, as the chitosan peak disappears (Fig. 6). For the other formulations, the results indicate that the incorporation of clay might not reinforce the chitosan matrix. Previous studies have highlighted that poorly dispersed clay nanoparticles can act as points of

stress concentration, leading to reduced resistance of the material [84]. For instance, VHS K shows a tensile strength of 0.59 MPa, while PS9 K shows 0.75 MPa, both of which are lower than K. In the case of L chitosan, the combination with clays leads a reduction in resistance for both types, BC-L and UC-L. Notably, the UC-L that showed the highest tensile strength among all formulations (1.21 MPa), when combined with PS9 shows a moderate tensile strength of 0.81 MPa, slightly better than VHS UC-L (0.67 MPa). For PE-derived chitosan, when combined with PS9 clay, BC-PE film shows a reduction in tensile strength to 0.24 MPa, suggesting a significant weakening effect from the clay, but the PS9 UC-PE film maintains a relatively high tensile strength (1.0 MPa). Overall, it can be deduced that PS9 clay tends to perform better than VHS in terms of maintaining or improving the tensile strength of C-C NFs, especially if we look at the best results obtained with chitosan from *H. illucens*, namely those using UC.

At first glance, this result contradicts expectations, as the combination of clays and polymers is often intended to enhance the mechanical

strength of the resulting nanocomposite [85]. However, the mere combination of clay and polymer is not sufficient to guarantee improved mechanical properties, as this largely depends on the interaction between the two components and the homogeneous dispersion of clay nanoparticles [64]. Similar studies have reported a deterioration in the mechanical strength of polymers following the addition of clays, attributing this to the presence of small clay agglomerates within the polymer matrix, which create points of fragility in the polymer network, concentrating mechanical stress in these areas and facilitating the film rupture [84].

### 3.8.2. Elongation at break

The results from the EAB test, reported in Fig. 9, provide key insights into the elasticity of films. These results indicate how much the films can stretch before breaking, offering a clear measure of their flexibility. Among the different chitosan formulations, the K consistently demonstrates superior elasticity, as evidenced by its high EAB values under all conditions. When no clay is present (C), K achieves an elongation of 107.86 %, and this value increases significantly when VHS is introduced, reaching 138.15 %, the highest value among all samples. Even when PS9 is added, K film remains highly elastic, with an elongation of 114.10 %. For *H. illucens* chitosan, films made from BC generally show lower elasticity compared to those made from UC. In this case, the addition of clay results in a marked decline in elasticity. For instance, BC-L has an EAB of 90.65 %, but this drops drastically when VHS is added, reaching only 62.56 %. A similar trend is observed for BC-PE and BC-A films. On the other hand, films made from UC exhibit much better performance in terms of elasticity: UC-L film shows an EAB of 104.40 %, while UC-PE and UC-A display similar values of 98.94 % and 95.50 %, respectively. In C-C NFs, the addition of PS9 to the UC performs better results: PS9 UC-PE achieves an elongation at break of 107.81 %, and PS9 UC-A reaches 106.04 %, values that are comparable to the performance of K. The PS9 clay, therefore, appears to act as a more effective plasticizer in UC films, enhancing their mechanical properties [86]. In terms of clay influence, there are clear differences between VHS and PS9. VHS generally tends to reduce the elasticity of the films, particularly in BC samples. For instance, BC-PE and BC-A films experience a significant drop in elongation at break when VHS is added, falling to 77.51 % and 73 %, respectively. Conversely, PS9 seems to have a more favorable effect on elasticity, particularly in UC-based films.

### 3.8.3. Adhesion test

In the adhesion test, the force required to separate the film from the gelatin substrate, which simulates skin, reveals the adhesive potential of the formulations intended for biomedical applications. The data, represented in Fig. 10, clearly show that films made from *H. illucens* chitosan have, in most cases, superior adhesive properties compared to commercial chitosan (K). The UC-L sample shows high adhesion properties (0.398 N), which is considerably better than that of K (0.146 N). This suggests that UC-L has a more flexible and perhaps better-interacting polymer structure, allowing it to form stronger bonds with the gelatin substrate. When considering the effect of clay, both VHS and PS9 show notable differences in how they influence the adhesion properties. In particular, the addition of VHS tends to reduce the adhesive strength of the films. For example, the adhesion of UC-L drops from 0.398 N (no clay) to 0.327 N when VHS is added. This trend is consistent across other chitosan sources (UC-PE and UC-A). The reduction in adhesion can be attributed to the interaction between VHS and the chitosan matrix, which likely stiffens the polymer and reduces its ability to interact effectively with the substrate. This phenomenon is consistent with the results found in other studies on nanocomposites, where clay particles can reduce the polymer's mobility and thus its ability to adhere to a surface [32].

PS9, on the other hand, seems to have a more favorable effect on adhesion, particularly in UC films. For instance, PS9 UC-PE shows a significant increase in adhesion, reaching 0.445 N, the highest adhesive value across all tested formulations. Similarly, PS9 UC-A also exhibits high adhesion (0.410 N). These results suggest that PS9 not only reinforces the polymer matrix but also enhances the film's ability to adhere to the surface. In contrast, BC films show lower adhesion overall, especially when VHS is added. For example, BC-A with VHS has a notably low adhesion of 0.092 N, indicating that the combination of bleaching and the addition of VHS creates a much stiffer and less interactive film. Even without clay, BC films tend to show lower adhesion values compared to UC, suggesting that the bleaching process itself affects the chitosan adhesive ability. Interestingly, the K performs poorly in adhesion tests relative to the other formulations. Its best result is observed when combined with VHS (0.207 N), but even this is significantly lower than the adhesive performance of the *H. illucens* chitosan formulations. This reinforces the idea that *H. illucens* chitosan, especially when used in combination with PS9, offers a superior alternative for

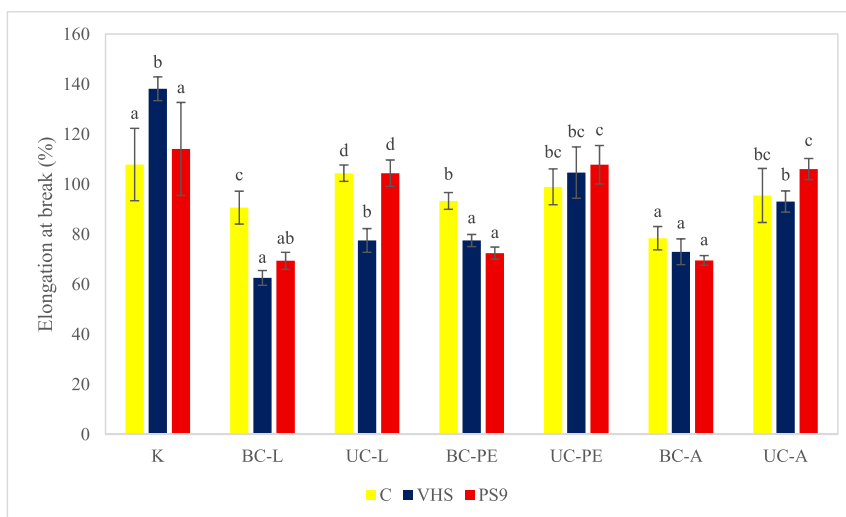


**Fig. 9.** EAB results expressed in % for each of the film formulations (mean  $\pm$  s.d.;  $n = 5$ ). The film samples are grouped into seven groups according to the type of chitosan used for film production (K, BC-L, UC-L, BC-PE, UC-PE, BC-A, UC-A). Within each group, the yellow bar (C) corresponds to the film produced with only chitosan, the blue bar (VHS) to the films containing montmorillonite, and the red bar (PS9) to those containing sepiolite. The statistical analysis presented in the graph was conducted separately for each biomass (K, L, PE, A). For the analysis comparing the results across all samples, please refer to the "Supporting Information" section. (For interpretation of the references to color in this figure legend, the reader is referred to the web version of this article.)

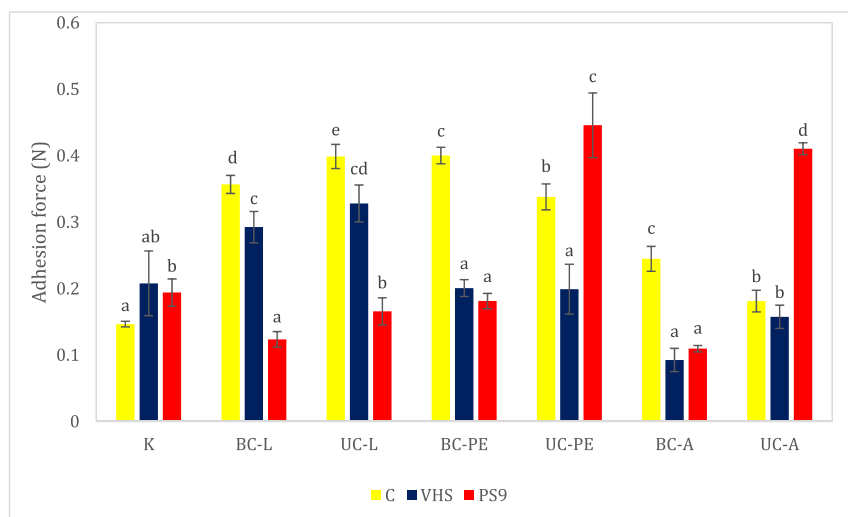


**Fig. 10.** Adhesion Test results expressed in N for each of the film formulations (mean  $\pm$  s.d.;  $n = 5$ ). The film samples are grouped into seven groups according to the type of chitosan used for film production (K, BC-L, UC-L, BC-PE, UC-PE, BC-A, UC-A). Within each group, the yellow bar (C) corresponds to the film produced with only chitosan, the blue bar (VHS) to the films containing montmorillonite, and the red bar (PS9) to those containing sepiolite. The statistical analysis presented in the graph was conducted separately for each biomass (K, L, PE, A). For the analysis comparing the results across all samples, please refer to the “Supporting Information” section. (For interpretation of the references to color in this figure legend, the reader is referred to the web version of this article.)

applications that require strong bioadhesion, such as wound dressings or drug delivery films.

#### 4. Conclusions

This study demonstrates that some of the films made with chitosan from *H. illucens* biomasses, especially UC-L, UC-PE, and UC-A, exhibit superior mechanical and thermal properties compared to K films. Among the tested films, the unbleached chitosan (UC) variants generally outperformed the bleached (BC) ones, suggesting that bleaching process is unnecessary to achieve optimal film properties and potentially detrimental for this type of formulation, simplifying production and reducing environmental impact. The addition of clay, especially sepiolite (PS9), improved the thermal stability and, in most cases, the mechanical properties as well, particularly in UC films. The enhancement of thermal stability is a critical parameter in both medical and cosmetic fields. The majority of commercially available biopolymers are not heat-resistant and tend to undergo thermal degradation. This inherent sensitivity significantly limits their suitability for essential processes such as sterilization, thereby restricting their practical applications in these fields. The films containing PS9 demonstrated better clay dispersion compared to VHS, likely due to stronger interactions between the clay particles and the polymer matrix. The wettability analysis indicated increased hydrophobicity upon clay addition, particularly with VHS, which could make the films more suitable for applications requiring moisture resistance, such as packaging, wound dressing, and drug delivery. Among the different types of chitosan tested, the one derived from A demonstrated the highest resistance to water, exhibiting the most hydrophobic behavior. In contrast, K was found to be the most hydrophilic, making it more susceptible to solubilization in aqueous environments. The films produced from BSF chitosan demonstrated superior hydrophobicity and, most notably, enhanced adhesiveness compared to those derived from K. The properties exhibited by these films are particularly well-suited for applications in the development of advanced wound and burn healing systems tailored for exudative conditions. Hydrophobicity represents a pivotal characteristic in such formulations, as hydrophilic films, when exposed to exudate, may undergo premature dissolution. This can compromise their functional integrity, reduce therapeutic efficacy, and alter the controlled release profile of incorporated active compounds. Moreover, the superior adhesiveness observed in these films facilitates

prolonged retention at the application site, thereby enhancing patient adherence to treatment protocols and supporting sustained therapeutic outcomes. In conclusion, this research highlights the potential of *H. illucens* as a sustainable source of chitosan for producing advanced biomaterials. Indeed, it has shown to be suitable for combination with other compounds, such as clays, allowing its properties to be modified as needed. In this case, the addition of clays led to changes in mechanical strength, thermal stability, and hydrophobicity of the chitosan films. Future research should focus on evaluating this formulation through *in vitro* and *in vivo* assays to comprehensively assess its potential for drug delivery, wound healing, antibacterial, and antioxidant activities. Additionally, it would be valuable to investigate its anti-inflammatory effects, biocompatibility with human tissues, and capacity to enhance cell regeneration. The synergistic interaction between chitosan and clay may further amplify these biological functions, positioning this formulation as a promising candidate for advanced biomedical applications.

#### CRediT authorship contribution statement

**Dolores Ianniciello:** Writing – review & editing, Writing – original draft, Methodology, Data curation. **Ada Peláez Montosa:** Writing – review & editing, Data curation. **Raquel de Melo Barbosa:** Writing – review & editing, Methodology. **Fátima García Villén:** Writing – review & editing, Data curation. **Rosanna Salvia:** Writing – review & editing, Data curation. **Carmen Scieuzo:** Data curation, Writing – review & editing. **César Viseras:** Writing – review & editing, Writing – original draft, Supervision, Methodology, Data curation, Conceptualization. **Patrizia Falabella:** Writing – review & editing, Writing – original draft, Supervision, Data curation, Conceptualization.

#### Declaration of Generative AI and AI-assisted technologies in the writing process

During the preparation of this work the authors used ChatGPT in order to improve readability and language. After using this tool/service, the authors reviewed and edited the content as needed and takes full responsibility for the content of the publication.

## Funding

This work was supported by University of Basilicata within the framework of “Sustainable biopackaging solutions from *Hermetia illucens* chitosan, proteins, and lipids (PACKILLUCENS)” within the “Partenariati estesi alle università, ai centri di ricerca, alle aziende per il finanziamento di progetti di ricerca di base”, and received funding from the European Union Next-GenerationEU (PIANO NAZIONALE DI RIPRESA E RESILIENZA (PNRR) - MISSIONE 4 COMPONENTE 2 INVESTIMENTO 1.3, PE00000003 – “ON FOODS - RESEARCH AND INNOVATION NETWORK ON FOOD AND NUTRITION SUSTAINABILITY, SAFETY AND SECURITY – WORKING ON FOODS”)- DD n. 1550 - 11.10.2022; University of Granada (authors are also thankful for the support offered by the Spanish Project PID2022-137603013-100 (Ministerio de Ciencia, Innovación y Universidades) and by the Italian Ministry of University and Research under Decree No. 1061—10/08/2021, through a Ph.D. scholarship (DOT208JXBA - 2) within the “National Operational Program Research and Innovation 2014–2020” (CCI 2014IT16M2OP005), FSE REACT-EU resources, Action IV.4 “Doctorates and research contracts on innovation topics” and Action IV.5 “Doctorates on green topics”.

## Declaration of competing interest

The authors declare that they have no known competing financial interests or personal relationships that could have appeared to influence the work reported in this paper.

## Appendix A. Supplementary data

Supplementary data to this article can be found online at <https://doi.org/10.1016/j.ijbiomac.2025.143496>.

## Data availability

The datasets used and/or analyzed during the current study are available from the corresponding author on reasonable request.

## References

- Precedence Research, Polymers Market Size, Share, Growth, Trends 2024–2032. <https://www.precedenceresearch.com/polymers-market>.
- A.J. Domb, N. Kumar, *Biodegradable Polymers in Clinical Use and Clinical Development*, John Wiley & Sons, 2011.
- A. Mtibe, M.P. Motloung, J. Bandyopadhyay, S.S. Ray, *Macromol. Rapid Commun.* 42 (15) (2021) 2100130, <https://doi.org/10.1002/marc.202100130>.
- S. Bhatia, *Natural Polymer Drug Delivery Systems: Nanoparticles, Plants, and Algae*, Springer, 2016, pp. 95–118, [https://doi.org/10.1007/978-3-319-41129-3\\_3](https://doi.org/10.1007/978-3-319-41129-3_3).
- C.C. Kandar, M.S. Hasnain, A.K. Nayak, *Advances and Challenges in Pharmaceutical Technology*, Academic Press, 2021, pp. 1–44, <https://doi.org/10.1016/B978-0-12-820043-8.00012->.
- R. Balart, D. Garcia-Garcia, V. Fombuena, L. Quiles-Carrillo, M.P. Arrieta, *Polymers* 13 (15) (2021) 2532, <https://doi.org/10.3390/polym13152532>.
- P.K. Dutta, D. Joydeep, V.S. Tripathi, *J. Sci. Ind. Res.* 63 (2004) 20–31.
- D. Elieh-Ali-Komi, M.R. Hamblin, *Int. J. Adv. Res.* 4 (2016) 411–427.
- M. Rinaudo, *Prog. Polym. Sci.* 31 (2006) 603–632, <https://doi.org/10.1016/j.procpolymsci.2006.06.001>.
- T. Hahn, E. Tafi, A. Paul, R. Salvia, P. Falabella, S. Zibek, *J. Chem. Technol. Biotechnol.* 95 (11) (2020) 2775–2795, <https://doi.org/10.1002/jctb.6533>.
- I. Aranz, A.R. Alcántara, M.C. Civera, C. Arias, B. Elorza, A. Heras Caballero, N. Acosta, *Polymers* 13 (19) (2021) 3256, <https://doi.org/10.3390/polym13193256>.
- M. Yadav, B. Kaushik, G.K. Rao, C.M. Srivastava, D. Vaya, *Carbohydr. Polym. Technol. Appl.* 5 (2023) 100323, <https://doi.org/10.1016/j.carpta.2023.100323>.
- X. Tao, Z. Wang, B. Ren, J. Li, T. Zhou, H. Tan, X. Niu, *J. Biol. Macromol.* 279 (2024) 134829, <https://doi.org/10.1016/j.ijbiomac.2024.134829>.
- A. Guarnieri, M. Triunfo, C. Scieuzo, D. Ianniciello, E. Tafi, T. Hahn, S. Zibek, R. Salvia, A. De Bonis, P. Falabella, *Sci. Rep.* 12 (1) (2022) 8084, <https://doi.org/10.1038/s41598-022-10423-5>.
- G.J. Tsai, W.H. Su, *JFP* 62 (3) (1999) 239–243, <https://doi.org/10.4315/0362-028X-62.3.239>.
- S. Mao, W. Sun, T. Kissel, *Adv. Drug Deliv. Rev.* 62 (1) (2010) 12–27, <https://doi.org/10.1016/j.addr.2009.08.004>.
- A. Ali, S. Ahmed, *Int. J. Biol. Macromol.* 109 (2018) 273–286, <https://doi.org/10.1016/j.ijbiomac.2017.12.078>.
- A. Bernkop-Schnürch, S. Dünnhaupt, *Eur. J. Pharm.* 81 (3) (2012) 463–469, <https://doi.org/10.1016/j.ejpb.2012.04.007>.
- T. Maschmeyer, R. Luque, M. Selva, *Chem. Soc. Rev.* 49 (13) (2020) 4527–4563, <https://doi.org/10.1039/c9cs00653b>.
- S.A. Siddiqui, S.N. Rahmadhia, S. Nair, S. Sabu, A. Ahmad, A. Sasidharan, *PSEP* (2024), <https://doi.org/10.1016/j.psep.2024.08.035>.
- Verified Market Research, Chitin and chitosan derivatives market size, share & forecast. <https://www.verifiedmarketresearch.com/product/chitin-and-chitosan-derivatives-market/>.
- C. Scieuzo, A. Franco, R. Salvia, M. Triunfo, N.F. Addeo, S. Vozzo, G. Piccolo, F. Bovera, A. Ritieni, A. Di Francia, A. Laginestra, E. Schmitt, P. Falabella, *Insect Sci.* 30 (4) (2023) 991–1010, <https://doi.org/10.1111/1744-7917.13155>.
- A. Franco, R. Rinaldi, F. Giglio, D. Ianniciello, A. Boschi, C. Scieuzo, R. Salvia, P. Falabella, *Entomol. Gen.* (2024) 813–831, <https://doi.org/10.1127/entomologia/2024/2651>.
- M. Triunfo, E. Tafi, A. Guarnieri, C. Scieuzo, T. Hahn, S. Zibek, R. Salvia, P. Falabella, *Cosmetics* 8 (2) (2021) 40, <https://doi.org/10.3390/cosmetics8020040>.
- E. Guzmán, F. Ortega, R.G. Rubio, *Cosmetics* 9 (5) (2022) 99, <https://doi.org/10.3390/cosmetics9050099>.
- R.A. Muzzarelli, M. Mattioli-Belmonte, A. Pugnali, G. Biagini, *Exs* 87 (1999) 251–264, [https://doi.org/10.1007/978-3-0348-8757-1\\_18](https://doi.org/10.1007/978-3-0348-8757-1_18).
- M.N.V. Ravi Kumar, *Bull. Mater. Sci.* 22 (1999) 905–915, <https://doi.org/10.1007/BF02745552>.
- G. Sandri, C. Aguzzi, S. Rossi, M.C. Bonferoni, G. Bruni, C. Boselli, A.I. Cornaglia, F. Riva, C. Viseras, C. Caramella, F. Ferrari, *Acta Biomater.* 57 (2017) 216–224, <https://doi.org/10.1016/j.actbio.2017.05.032>.
- O. Felt, P. Buri, R. Gurny, *Drug Dev. Ind. Pharm.* 24 (11) (1998) 979–993, <https://doi.org/10.3109/03639049809089942>.
- K. Jaferník, A. Ładniak, E. Blicharska, K. Czarnek, H. Ekiert, A.E. Więcek, A. Szopa, *Molecules* 28 (4) (2023) 1963, <https://doi.org/10.3390/molecules28041963>.
- C. Viseras, P. Cerezo, R. Sanchez, I. Salcedo, C. Aguzzi, *Appl. Clay Sci.* 48 (3) (2010) 291–295, <https://doi.org/10.1016/j.clay.2010.01.007>.
- I. Salcedo, C. Aguzzi, G. Sandri, M.C. Bonferoni, M. Mori, P. Cerezo, R. Sanchez, C. Viseras, C. Caramella, *Appl. Clay Sci.* 55 (2012) 131–137, <https://doi.org/10.1016/j.clay.2011.11.006>.
- M. Hnamte, A.K. Pulikkal, *Chemosphere* 307 (2022) 135869, <https://doi.org/10.1016/j.chemosphere.2022.135869>.
- F.S. Ebnerasool, N.M. Kazemi, *Anal. Methods Environ. Chem. J.* 2 (2) (2019) 5–12, <https://doi.org/10.24200/amecj>.
- C. Viseras, C. Aguzzi, P. Cerezo, M.C. Bedmar, *Mater. Sci. Technol.* 24 (9) (2008) 1020–1026, <https://doi.org/10.1179/174328408X341708>.
- C. Aguzzi, P. Capra, C. Bonferoni, P. Cerezo, I. Salcedo, R. Sánchez, C. Caramella, C. Viseras, *Appl. Clay Sci.* 50 (1) (2010) 106–111, <https://doi.org/10.1016/j.clay.2010.07.011>.
- C. Aguzzi, P. Cerezo, I. Salcedo, R. Sánchez, C. Viseras, *Mater. Technol.* 25 (3–4) (2010) 205–211, <https://doi.org/10.1179/175355510X12723642365566>.
- G. Sandri, M.C. Bonferoni, F. Ferrari, S. Rossi, C. Aguzzi, M. Mori, P. Grisoli, P. Cerezo, M. Tenci, C. Viseras, C. Caramella, *Carbohydr. Polym.* 102 (2014) 970–977, <https://doi.org/10.1016/j.carbpol.2013.10.029>.
- G. Sandri, A. Faccendini, M. Longo, M. Ruggeri, S. Rossi, M.C. Bonferoni, D. Miele, A. Prina-Mello, C. Aguzzi, C. Viseras, F. Ferrari, *Pharmaceutics* 12 (2) (2020) 179, <https://doi.org/10.3390/pharmaceutics12020179>.
- E. Bianchi, B. Viganì, C. Viseras, F. Ferrari, S. Rossi, G. Sandri, *Pharmaceutics* 14 (6) (2022) 1127, <https://doi.org/10.3390/pharmaceutics14061127>.
- A.A. Tavares, M.D.M. Macêdo, P.H.C. de Lima, R.C. Barbosa, W.J.B. Sousa, C.J. de Farias Braz, M.F. de Sousa, C.M.G.P. Diniz, M.V.L. Fook, S.M. de Lima Silva, *Res. Soc. Dev.* 11 (1) (2022) e25911124684, <https://doi.org/10.33448/rsd-v11i1.24684>.
- C.L. Pérez Gutiérrez, A. Di Michele, C. Pagano, D. Puglia, F. Luzi, T. Beccari, M. R. Ceccarini, S. Primavilla, A. Valiani, C. Vicino, M. Ricci, C. Viseras, L. Perioli, *Pharmaceutics* 15 (8) (2023) 2057, <https://doi.org/10.3390/pharmaceutics15082057>.
- J. Dutta, N. Devi, *Int. J. Biol. Macromol.* 186 (2021) 244–254, <https://doi.org/10.1016/j.ijbiomac.2021.07.020>.
- European Pharmacopoeia (Ph. Eur. 11th; Volume III), *Magnesium Trisilicate monograph*, Council of Europe, Strasbourg, 2023.
- United States Pharmacopoeia and National Formulary (USP 42 – NF 37; Volume 3), *United States Pharmacopoeial Convention*, Rockville, 2019.
- M. Triunfo, E. Tafi, A. Guarnieri, R. Salvia, C. Scieuzo, T. Hahn, S. Zibek, A. Gagliardini, L. Panariello, M.B. Coltelli, A. De Bonis, P. Falabella, *Sci. Rep.* 12 (1) (2022) 6613, <https://doi.org/10.1038/s41598-022-10423-5>.
- U. Siemann, *Scattering methods and the properties of polymer materials*, Springer Berlin Heidelberg, Berlin, Heidelberg, 2005, pp. 1–14.
- European Pharmacopoeia 8.0, *Wettability of Porous Solids Including Powders vol. I*, 2014 p.2.9.45.
- S.I. Park, Y. Zhao, *J. Agric. Food Chem.* 52 (7) (2004) 1933–1939, <https://doi.org/10.1021/jf034612p>.
- T. Martínez Rodríguez, C. Valentino, F.R. Rodríguez Pozo, P. Hernández Benavides, F. Arrebola Vargas, J.M. Paredes, C.I. Sainz-Díaz, G.R. Iglesias, S. Rossi, G. Sandri, M.M.M. Perez, C. Aguzzi, *J. Funct. Biomater.* 15 (3) (2024) 69, <https://doi.org/10.3390/jfb15030069>.
- S. Alaei, Y. Omid, H. Omidian, *Eur. J. Pharm. Sci.* 166 (2021) 105965, <https://doi.org/10.1016/j.ejps.2021.105965>.

- [52] J.B. Olivato, J. Marini, F. Yamashita, E. Pollet, M.V.E. Grossmann, L. Avérous, *Mater. Sci. Eng. C* 70 (2017) 296–302, <https://doi.org/10.1016/j.msec.2016.08.077>.
- [53] J.E. Kasmani, A. Samariha, *Bioresources* 16 (3) (2021) 6281, <https://doi.org/10.15376/biores.16.3.6281-6291>.
- [54] I. Leceta, P. Guerrero, K. De La Caba, *Carbohydr. Polym.* 93 (1) (2013) 339–346, <https://doi.org/10.1016/j.carbpol.2012.04.031>.
- [55] M. Darder, M. Colilla, E. Ruiz-Hitzky, *Chem. Mater.* 15 (20) (2003) 3774–3780, <https://doi.org/10.1021/cm0343047>.
- [56] M. Darder, M. López-Blanco, P. Aranda, A.J. Aznar, J. Bravo, E. Ruiz-Hitzky, *Chem. Mater.* 18 (6) (2006) 1602–1610, <https://doi.org/10.1021/cm0523642>.
- [57] A. López-Galindo, C. Viseras, *Interface Science and Technology* 1, 2004, pp. 267–289, [https://doi.org/10.1016/S1573-4285\(04\)80044-9](https://doi.org/10.1016/S1573-4285(04)80044-9).
- [58] F. Bergaya, G. Lagaly, *Dev. Clay Sci.* 1 (2006) 1–18, [https://doi.org/10.1016/S1572-4352\(05\)01001-9](https://doi.org/10.1016/S1572-4352(05)01001-9).
- [59] A. Borrego-Sánchez, R. Sánchez-Espejo, F. García-Villén, C. Viseras, C.I. Sainz-Díaz, *Pharmaceutics* 12 (10) (2020) 914, <https://doi.org/10.3390/pharmaceutics12100914>.
- [60] C. Branca, G. D'Angelo, C. Crupi, K. Khouzami, S. Rifici, G. Ruello, U. Wanderlingh, *Polymer* 99 (2016) 614–622, <https://doi.org/10.1016/j.polymer.2016.07.086>.
- [61] A.B.D. Nandiyanto, R. Oktiani, R. Ragadhita, *Indonesian Journal of Science and Technology* 4 (1) (2019) 97–118.
- [62] F. García-Villén, A. Faccendini, C. Aguzzi, P. Cerezo, M.C. Bonferoni, S. Rossi, P. Grisoli, M. Ruggeri, F. Ferrari, G. Sandri, C. Viseras, Montmorillonite-norfloracin nanocomposite intended for healing of infected wounds, *Int. J. Nanomedicine* (2019) 5051–5060, <https://doi.org/10.2147/IJN.S208713>.
- [63] F. García-Villén, R. Sánchez-Espejo, A. López-Galindo, P. Cerezo, C. Viseras, *Appl. Clay Sci.* (2020) 105772, <https://doi.org/10.1016/j.clay.2020.105772>.
- [64] M. Almazrouei, T. El Samad, I. Janajreh, *Energy Procedia* 142 (2017) 1699–1705, <https://doi.org/10.1016/j.egypro.2017.12.552>.
- [65] V.Y. Mena-Cervantes, R. Hernández-Altamirano, A. Tiscareño-Ferrer, *Environ. Sci. Pollut. Res. Int.* 27 (2020) 28500–28509, <https://doi.org/10.1007/s11356-019-07287-0>.
- [66] J. Nunthanid, S. Puttipipatkachorn, K. Yamamoto, G.E. Peck, *Drug Dev. Ind. Pharm.* 27 (2) (2001) 143–157, <https://doi.org/10.1081/DDC-100000481>.
- [67] L. Balau, G. Lisa, M.I. Popa, V. Tura, V. Melnig, *Cent. Eur. J. Chem.* 2 (2004) 638–647, <https://doi.org/10.2478/BF02482727>.
- [68] P.Z. Hong, S.D. Li, C.Y. Ou, C.P. Li, L. Yang, C.H. Zhang, *J. Appl. Polym. Sci.* 105 (2) (2007) 547–551, <https://doi.org/10.1002/app.25920>.
- [69] J. Kerwald, A.G. De Mitri, J.A. de Moura Delezuk, G.J. de Castilho, M.M. Beppu, *Biomed. Mater. & Dev.* 1 (1) (2023) 213–233, <https://doi.org/10.1007/s44174-022-00021-4>.
- [70] Q. Luo, Y. Wang, Q. Han, L. Ji, H. Zhang, Z. Fei, Y. Wang, *Carbohydr. Polym.* 209 (2019) 266–275, <https://doi.org/10.1016/j.carbpol.2019.01.030>.
- [71] D.F. Xie, V.P. Martino, P. Sangwan, C. Way, G.A. Cash, E. Pollet, K.M. Dean, P. J. Halley, L. Avérous, *Polymer* 54 (14) (2013) 3654–3662, <https://doi.org/10.1016/j.polymer.2013.05.017>.
- [72] A. Osorio-Madrado, L. David, S. Trombotto, J.M. Lucas, C. Peniche-Covas, A. Domard, *Biomacromolecules* 11 (5) (2010) 1376–1386, <https://doi.org/10.1021/bm1001685>.
- [73] K. Ogawa, T. Yui, M. Miya, *Biosci. Biotechnol. Biochem.* 56 (6) (1992) 858–862, <https://doi.org/10.1271/bbb.56.858>.
- [74] R. Rafiee, R. Shahzadi, *Polym. Compos.* 40 (2) (2019) 431–445, <https://doi.org/10.1002/pc.24725>.
- [75] E. Grządka, E. Godek, T.A. Le, U. Maciolek, M. Galaburda, J. Orzeł, T. Leskinen, T. P. Huynh, *Sep. Purif. Technol.* 348 (2024) 127671, <https://doi.org/10.1016/j.seppur.2024.127671>.
- [76] J.J. Kaschuk, Y. Al Haj, J.V. Garcia, A. Kamppinen, O.J. Rojas, T. Abitbol, K. Miettunen, J. Vapaavuori, *Carbohydr. Polym.* 332 (2024) 121877, <https://doi.org/10.1016/j.carbpol.2024.121877>.
- [77] X. Nie, H. Shi, F. Wang, C. You, D. Zhang, Z. Xiao, X. Li, *Food Hydrocoll.* 157 (2024) 110436, <https://doi.org/10.1016/j.foodhyd.2024.110436>.
- [78] H.M. Frühauf, M. Stöckl, D. Holtmann, *Vol.* 22, No. 6, 2022, pp. 464–470.
- [79] F.Z. Semlali Aouragh Hassani, K. El Bourakadi, N. Merghoub, A. El Kacem Qaiss, R. Bouhfid, *Int. J. Biol. Macromol.* 148 (2020) 316–323, <https://doi.org/10.1016/j.ijbiomac.2020.01.092>.
- [80] N.E. Suyatma, L. Tighzert, A. Copinet, V. Coma, *J. Agric. Food Chem.* 53 (10) (2005) 3950–3957, <https://doi.org/10.1021/jf048790>.
- [81] P. Chen, F. Xie, F. Tang, T. McNally, *Eur. Polym. J.* 13 (4) (2021) 571, <https://doi.org/10.3390/polym13040571>.
- [82] P. Sim, Y. Song, S. Abraham, S. Garg, *J. Drug Deliv. Sci. Tec.* 89 (2023) 105027, <https://doi.org/10.1016/j.jddst.2023.105027>.
- [83] L. Wang, Y. Luo, Y. Song, X. He, T. Xu, X. Zhang, *ACS Nano* 18 (4) (2024) 3468–3479, <https://doi.org/10.1021/acsnano.3c10766>.
- [84] I. Abdurrahim Kusmono, *Heliyon* 5 (8) (2019), <https://doi.org/10.1016/j.heliyon.2019.e02342>.
- [85] Y. Rao, J.M. Pochan, *Macromolecules* 40 (2) (2007) 290–296, <https://doi.org/10.1021/ma061445w>.
- [86] A. Giannakas, K. Grigoriadi, A. Leontiou, N.M. Barkoula, A. Ladavos, *Carbohydr. Polym.* 108 (1) (2014) 103–111, <https://doi.org/10.1016/j.carbpol.2014.03.019>.